Cerebral Cortex, January 2017;27: 146–161

doi: 10.1093/cercor/bhw361
Advance Access Publication Date: 1 December 2016
Original Article

ORIGINAL ARTICLE

The Cytoarchitecture of Domain-specific Regions in Human High-level Visual Cortex

Kevin S. Weiner[1,†], Michael A. Barnett[1,†], Simon Lorenz[2], Julian Caspers[2,3], Anthony Stigliani[1], Katrin Amunts[2,4,5], Karl Zilles[2,5,6], Bruce Fischl[7,8] and Kalanit Grill-Spector[1,9]

[1]Department of Psychology, Stanford University, Stanford, CA 94305, USA, [2]Institute of Neurosciences and Medicine (INM-1), Research Centre Jülich, 52428 Jülich, Germany, [3]Department of Diagnostic and Interventional Radiology, Medical Faculty, University of Düsseldorf, 40225 Düsseldorf, Germany, [4]Cécile and Oskar Vogt Institute for Brain Research, Heinrich-Heine University of Düsseldorf, 40225 Düsseldorf, Germany, [5]JARA-BRAIN, Jülich-Aachen Research Alliance, 52428 Jülich, Germany, [6]Department of Psychiatry, Psychotherapy and Psychosomatics, RWTH Aachen University, 52062 Aachen, Germany, [7]Martinos Center for Biomedical Imaging and Department of Radiology, Harvard Medical School, Massachusetts General Hospital, Boston, MA 02114, USA, [8]Computer Science and Artificial Intelligence Laboratory, MIT EECS/HST, Massachusetts Institute of Technology, Cambridge, MA 02139, USA and [9]Stanford Neurosciences Institute, Stanford University, Stanford, CA 94305, USA

Address correspondence to Kevin S. Weiner, Department of Psychology, Stanford University, Stanford, CA 94305, USA. Email: kweiner@stanford.edu; Kalanit Grill-Spector, Department of Psychology, Stanford University, Stanford, CA 94305, USA. Email: kalanit@stanford.edu

[†]Co first authors.

Abstract

A fundamental hypothesis in neuroscience proposes that underlying cellular architecture (cytoarchitecture) contributes to the functionality of a brain area. However, this hypothesis has not been tested in human ventral temporal cortex (VTC) that contains domain-specific regions causally involved in perception. To fill this gap in knowledge, we used cortex-based alignment to register functional regions from living participants to cytoarchitectonic areas in ex vivo brains. This novel approach reveals 3 findings. First, there is a consistent relationship between domain-specific regions and cytoarchitectonic areas: each functional region is largely restricted to 1 cytoarchitectonic area. Second, extracting cytoarchitectonic profiles from face- and place-selective regions after back-projecting each region to 20-μm thick histological sections indicates that cytoarchitectonic properties distinguish these regions from each other. Third, some cytoarchitectonic areas contain more than 1 domain-specific region. For example, face-, body-, and character-selective regions are located within the same cytoarchitectonic area. We summarize these findings with a parsimonious hypothesis incorporating how cellular properties may contribute to functional specialization in human VTC. Specifically, we link computational principles to correlated axes of functional and cytoarchitectonic segregation in human VTC, in which parallel processing across domains occurs along a lateral–medial axis while transformations of information within domain occur along an anterior–posterior axis.

Key words: brain map, cytoarchitecture, fusiform body area (FBA), fusiform face area (FFA), parahippocampal place area (PPA), visual word form area (VWFA)

Introduction

Human ventral temporal cortex (VTC) contains functional regions that are selective for specific domains such as faces (Puce et al. 1995; Kanwisher et al. 1997; Grill-Spector et al. 2004; Weiner and Grill-Spector 2010), places (Epstein and Kanwisher 1998), words (Cohen et al. 2000), and bodies (Peelen and Downing 2005a). These regions are also causally involved in the perception of domain-specific information (Gaillard et al. 2006; Parvizi et al. 2012; Megevand et al. 2014; Rangarajan et al. 2014). Interestingly, the anatomical location of these regions is reproducible across people (Peelen and Downing 2005a, 2005b; Spiridon et al. 2006; Weiner and Grill-Spector 2010; Nasr et al. 2011; Julian et al. 2012; Grill-Spector and Weiner 2014) and even predictable from cortical folding alone (Glezer and Riesenhuber 2013; Grill-Spector and Weiner 2014). Recent evidence indicates that anatomical features such as white matter (Saygin et al. 2012; Yeatman et al. 2012; Gomez et al. 2015; Osher et al. 2016; Wandell 2016; Weiner et al. 2016) and myelination (Glasser and Van Essen 2011) contribute to the consistent cortical location of functional regions especially for the large-scale positioning of face-selective regions on the lateral fusiform gyrus (FG) and of place-selective regions in the collateral sulcus (CoS; Glasser and Van Essen 2011; Saygin et al. 2012; Gomez et al. 2015).

However, a long-standing and fundamental hypothesis in neuroscience is that differences in the microarchitecture of cell bodies across cortical layers (referred to as cytoarchitecture) also contribute to the cortical location and functionality of brain regions (Brodmann 1909; von Economo and Koskinas 1925; Hubel and Wiesel 1977; Van Essen et al. 1992; Zilles and Amunts 2010; Amunts and Zilles 2015). This hypothesis predicts that cortical regions in human VTC that process information related to different domains would be located within different cytoarchitectonic areas. This hypothesis has not been tested for 2 main reasons. First, while the correspondence between cytoarchitecture and functional regions has been examined in non-human primates (typically macaques; Gross et al. 1972; Van Essen and Zeki 1978; Boussaoud et al. 1991; Zangenehpour and Chaudhuri 2005; Borra et al. 2010), the FG, which is a large macroanatomical component of VTC (Weiner and Zilles 2016), is a hominoid-specific gyrus that macaques do not have. Thus, understanding if and how underlying cytoarchitectonics contribute to the functional organization of the FG—and human VTC more broadly—necessitates measurements in humans. Second, only recently, observer-independent cytoarchitectonic techniques have revealed a microstructural heterogeneity of human VTC consisting of 4 cytoarchitectonic areas spanning the FG and nearby sulci (Caspers et al. 2013; Lorenz et al. 2015). The identification of these cytoarchitectonic areas generates a new opportunity to examine the correspondence between the functional and cytoarchitectonic heterogeneity of human VTC for the first time.

Understanding and quantifying the relationship between cytoarchitectonic areas and functional regions of human VTC in individual brains requires relating functional magnetic resonance imaging (fMRI) data at a macroscale (millimeters to centimeters) in living participants to cytoarchitectonic data at a microscale (microns) in postmortem (PM) brains. Prior studies successfully achieved this goal in early visual cortex by leveraging the tight relationship between both types of data and cortical folding using cortex-based alignment (CBA) (Fischl et al. 2008; Hinds et al. 2009). Since there is a tight relationship between both types of data and cortical folding in VTC (Weiner et al. 2014; Lorenz et al. 2015), we applied similar techniques in this study. In brief (Fig. 1; Materials and Methods), we registered cytoarchitectonic areas defined in histological slices of PM brains to a common brain using CBA to generate probabilistic maps of cytoarchitectonic regions of interest (cROIs). Then, we used CBA to register probabilistic cROIs to functional regions of interest (fROIs) from individual living participants and quantified the correspondence between cytoarchitectonic areas and functional regions. Crucially, the implementation of this analysis pipeline in the reverse order also enables the extraction of cytoarchitectonic profiles from fROIs by registering and projecting probabilistic fROIs to individual histological sections of PM brains.

Using this novel approach, we examined the relationship between domain-specific regions and cytoarchitectonic areas of human VTC. Our data indicate that there is a consistent relationship between domain-specific regions and cytoarchitectonic areas: each functional region is largely restricted to 1 cytoarchitectonic area. However, this relationship is not bidirectional, as

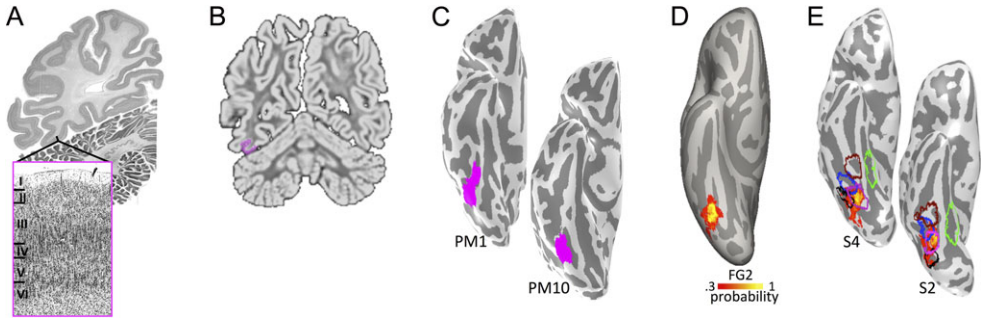

Figure 1. Relating the cytoarchitectonic and functional organization of VTC. (*A*) Observer-independent methods identify cROIs in stained histological sections from PM brains. (*B*) cROIs are projected from histological slices to anatomical T1-weighted images (T1s). (*C*) cROIs are projected from anatomical T1s to the cortical surface reconstruction of each individual and then to the FreeSurfer average brain using CBA. (*D*) Maximum probability maps (MPMs) of cROIs on the FreeSurfer average brain are determined from 10 PM brains. (*E*) The MPM of each cROI is projected to the cortical surface of each in vivo participant and compared with fROIs (outlines) in individual brains.

some cytoarchitectonic areas contain more than 1 domain-specific region. These findings support a new hypothesis suggesting what computational principles may explain the orderly but complex relationship between functional regions and cytoarchitectonic areas of human VTC.

Materials and Methods

Definitions of functional regions and cytoarchitectonic areas were done by independent researchers—researchers defining functional regions were blind to cytoarchitectonic definitions and vice versa. Data collection, analyses, and definitions of fROIs of in vivo data were done by K.W., A.S., M.B., and K.G-.S. at Stanford University. Data collection, analysis of PM data, and definition of cROIs were done at the Institute of Neuroscience and Medicine (INM-1), Research Centre Jülich, by J.C., S.L., K.A., and K.Z.

Participants of the In Vivo Study

Twelve right-handed participants (5 female, ages 19–44 years) with normal or corrected-to-normal vision were recruited from Stanford University for the functional mapping experiment, which was used to identify high-level visual regions in human VTC. Procedures were approved by the Stanford Internal Review Board on human subjects research.

In Vivo Data Acquisition and Analyses

Anatomical Scans and Analyses

Scanning. A high-resolution anatomical volume of the whole brain was acquired using a 3 T GE Discovery MR750 scanner (T1-weighted BRAVO pulse sequence; resolution: 1 mm × 1 mm × 1 mm, TI = 450 ms, flip angle = 12°, 1 NEX, FOV = 240 mm).

Cortical surface reconstruction. Anatomical volumes were aligned to the AC-PC plane. Using a combination of automated (FreeSurfer: http://surfer.nmr.mgh.harvard.edu) and manual segmentation tools (ITK-SNAP: http://www.itksnap.org/pmwiki/pmwiki.php), each anatomical volume was segmented to separate gray from white matter, from which we reconstructed the cortical surface for each participant (Wandell et al. 2000). These cortical surface reconstructions were used in both mrVista and FreeSurfer.

Functional Scans and Analyses

Data acquisition. Participants were scanned using a custom-built phase-array, 32-channel head coil. We acquired 34 slices covering occipitotemporal cortex (resolution: 2.4 mm × 2.4 mm × 2.4 mm; one-shot T2*-sensitive gradient echo acquisition sequence: FOV = 192 mm, TE = 30 ms, TR = 2000 ms, and flip angle = 77°).

Functional localizer. Two sessions of fMRI data were collected from each participant on different days. On the first day, 10 runs of an fMRI functional localizer experiment from Stigliani et al. (2015) were collected. Each run contained blocks of different images from 5 different categories: faces (adult and child faces), places (corridors and houses), bodies (limbs and headless bodies), characters (numbers, pseudowords), and objects (cars and guitars). Each run contained images presented at different rates (either 1, 2, 4, or 8 Hz). Stimulus trials were counterbalanced with blank baseline trials. In each run, stimuli were shown at one rate. The order of runs at different rates was counterbalanced across participants. The same set of 1440 images was shown across all rates, but images did not repeat within a rate. Participants conducted an oddball task during which they fixated on a central dot and detected an oddball phase scrambled image that occurred randomly in a block. The incidence of the oddball image was 0, 1, or 2 times per block. We chose this task as it keeps participants engaged during the experiment and is frequently used in studies of human VTC (Kanwisher et al. 1997; Gauthier et al. 2000; Glezer et al. 2009; Weiner and Grill-Spector 2010, 2011; Stigliani et al. 2015. Additionally, responses in VTC in the oddball task are similar to other tasks that require explicit processing of the visual images such as categorization tasks (Weiner and Grill-Spector 2010; Weiner et al. 2010), 1 or 2-back tasks (Weiner and Grill-Spector 2010; Weiner et al. 2010; Bugatus et al. 2015), or selective attention (Bugatus et al. 2015, 2016).

On the second day, participants participated in 2 runs totaling 11 minutes of the 1 Hz localizer experiment with the same stimuli and task. The purpose of the second experiment was to extract response amplitudes from fROIs using independent data (Fig. 2).

Data analysis. Data were analyzed with MATLAB using mrVista software (http://github.com/vistalab) as in our prior publications (Weiner and Grill-Spector 2010; Stigliani et al. 2015).

Time series processing. Functional data of each session were motion corrected using an affine transformation (Nestares and Heeger 2000). Time series data were processed with a temporal high-pass filter using a 1/20 Hz cutoff and then converted to percentage signal change by dividing the time series of each voxel by its mean intensity. We estimated blood oxygen level–dependent (BOLD) response amplitudes for each condition with a general linear model (GLM) applied to the time series of each voxel using as predictors the experimental conditions convolved with the hemodynamic impulse response function in SPM (http://www.fil.ion.ucl.ac.uk/spm/). Data were not spatially smoothed.

Functional regions of interest. FROIs were defined in individual participants from the functional localizer using anatomical and functional criteria (Weiner and Grill-Spector 2010, 2012; Stigliani et al. 2015). A common threshold ($t > 3$, voxel level) was used to define all regions across all participants. Since the cytoarchitectonic ROIs (described in the next section) are located in the occipitotemporal sulcus (OTS), FG, and CoS, we restricted our definition of fROIs to these anatomical regions.

As in our prior publications (Weiner and Grill-Spector 2010, 2012; Stigliani et al. 2015), we identified 2 face-selective ROIs (faces > others) bilaterally on the posterior (pFus-faces, $N = 12$) and mid (mFus-faces, $N = 12$) FG; pFus-faces is often referred to as FFA-1 and mFus-faces as FFA-2, where FFA refers to the fusiform face area (Kanwisher et al. 1997).

Between mFus-faces and pFus-faces, we identified a body-selective region (bodies and limbs > others) in the OTS ($N = 12$), which is also referred to as the fusiform body area (FBA; Peelen and Downing 2005a, 2005b; Schwarzlose et al. 2005).

As in our prior publications, we also identified 2 character-selective ROIs (characters > others; Stigliani et al. 2015) within the left hemisphere on the posterior (pOTS-chars, $N = 12$) and mid (mOTS-chars, $N = 10$) OTS. These ROIs are also referred to as VWFA-1 and VWFA-2, respectively (Stigliani et al. 2015), where VWFA refers to the visual word form area (Cohen et al. 2000; Ben-Shachar et al. 2011; Dehaene and Cohen 2011). In the right hemisphere, we also report data from pOTS-chars/VWFA-1

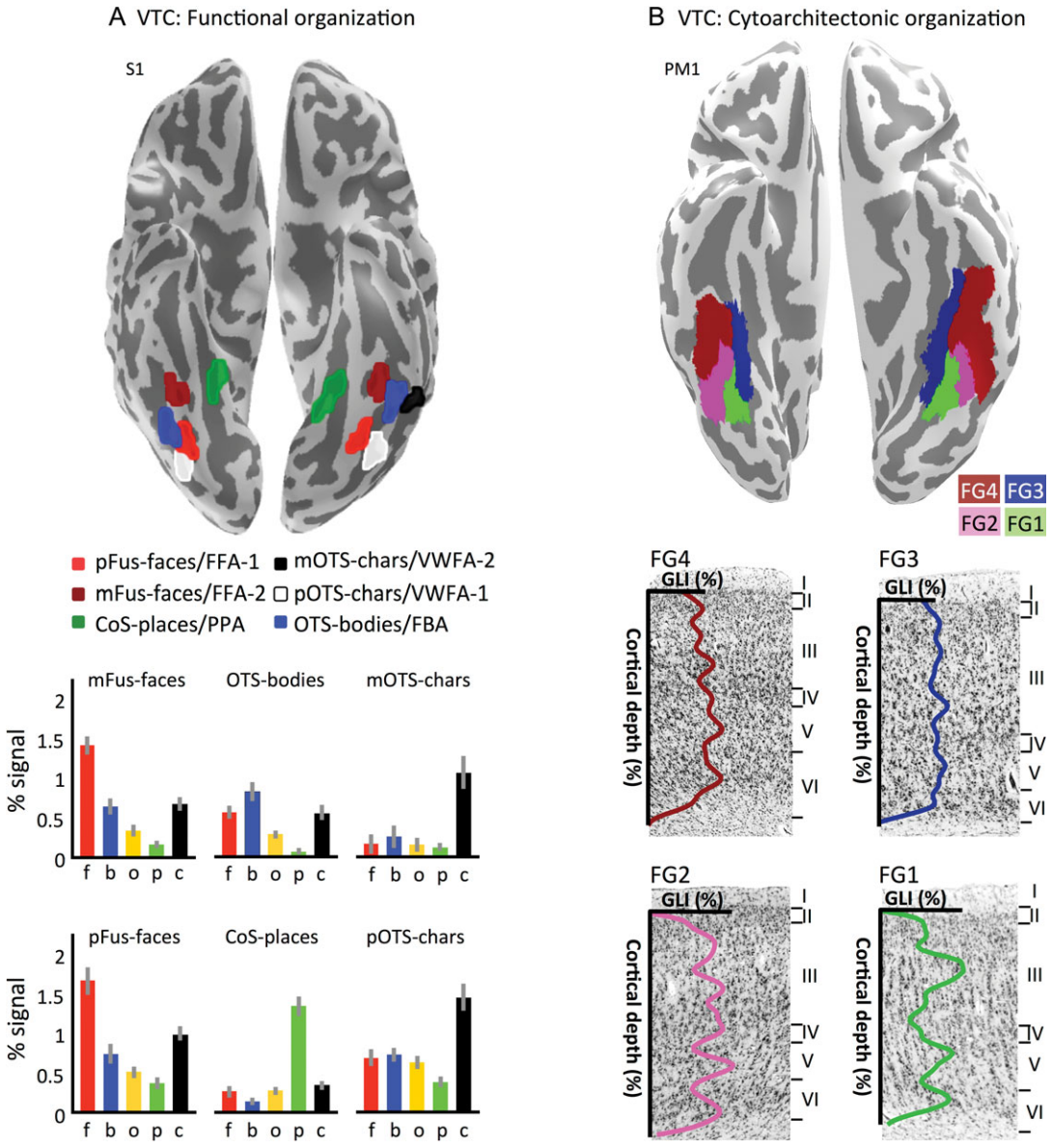

Figure 2. The definition and characteristics of functional regions and cytoarchitectonic areas in human VTC. (*A*) Functional organization of category-selective fROIs. *Top:* fROIs in an example subject (S1). *Bottom:* independent analysis of mean ± standard error of the mean of the amplitude of response to adult and child faces (f), bodies and limbs (b), cars and guitars (objects, o), corridors and buildings (places, p), and pseudowords and numbers (characters, c) in each fROI. Data are averaged across 12 subjects bilaterally for all fROIs, except mOTS-chars/VWFA-2, which includes data from the left hemisphere of 10 subjects. (*B*) Cytoarchitectonic areas in human VTC in an example PM subject. *Top:* cROIs in the FG and adjacent sulci in an example PM subject. Note that the medial cytoarchitectonic areas FG1 and FG3 encompass both the medial aspect of the FG and the CoS and the lateral cytoarchitectonic areas FG2 and FG4 encompass both the lateral FG and OTS. *Bottom:* example histological slices illustrating the representative cytoarchitectonic structure of FG1–FG4. *Acronyms:* pFus: posterior fusiform; mFus: mid-fusiform; pOTS: posterior occipitotemporal sulcus. mOTS: mid occipitotemporal sulcus.

($N = 12$), but not mOTS-chars/VWFA-2, as we were able to identify VWFA-2 in only 2 participants within the right hemisphere.

Finally, we identify a place-selective ROI (places > others) within the CoS ($N = 12$), corresponding to the parahippocampal place area (PPA; Epstein and Kanwisher, 1998). CoS-places/PPA has been recently parcellated into separate posterior and anterior components based on functional connectivity and weaker selectivity in the posterior compared with the anterior portion (Baldassano et al. 2013; Silson et al. 2015). Our analyses focus on the anterior CoS-places/PPA because this cortical location is the most consistent across participants and is predictive of clusters exhibiting the highest place-selectivity in over 500 participants (Weiner et al. Under review). Nevertheless, additional analyses show weakly place-selective voxels in FG1 (Supplementary Fig. 2).

Independent analysis of functional responses. Individual data from day 2 were aligned to each participant's high-resolution anatomical brain volume. Using fROIs defined in day 1, we extracted response amplitudes to faces, objects, bodies, places, and characters from day 2. Response amplitudes from each fROI were averaged across the 12 participants (Fig. 2A, bottom).

PM Data Acquisition and Analysis

Histological analyses were performed on eleven PM brains (ages 37–85, 6 females), which had no history of neurological or psychiatric disease (with exception of 1 individual with transitory motor disease). These were the same brains used in prior cytoarchitectonic studies (Caspers et al. 2013; Lorenz et al. 2015). Nine of the PM brains were shared across the Caspers and Lorenz studies (see table 1 in each of these studies), and each cytoarchitectonic area was defined in 10 PM brains (5 females). All PM brains came from the body donor program of the Institute of Anatomy, University of Dusseldorf; all procedures were approved and in alignment with the program guidelines (Amunts et al. 2000).

Scanning

PM brains were scanned on a Siemens 1.5 T Scanner (Erlangen, Germany). Brains were removed from the subject's skull 8–24 h after death and then fixated in 4% formalin or Bodian's fixative for at least 6 months. A high-resolution anatomical volume of the whole fixed brain was acquired using a T1-weighted 3D-FLASH sequence (TR = 40 ms, flip angle = 40°, TE = 5 ms).

Histological Processing

Detailed methods of histological processing have been published previously (Amunts et al. 2000; Caspers et al. 2013; Lorenz et al. 2015). Briefly, the fixated brains were embedded in paraffin, serially sectioned in coronal sections (20 μm thick), and cell bodies were stained using the Merker-method (Amunts et al. 2000). This method yields a high contrast between cell bodies (black) and the neuropil (unstained). 3D reconstructions of the histological sections were computed using 1) the 3D-MRI volume of each brain, 2) images of the paraffin block face for precise alignment of the histological sections, and 3) digitized images of the cell body–stained sections.

Definition of Cytoarchitectonic Regions

FG1, FG2, FG3, and FG4. FG1 and FG2 were defined by Caspers et al. (2013), and FG3 and FG4 were defined by Lorenz et al. (2015) from 20-μm thick sections of 10 PM brains using a statistically testable, quantitative, and observer-independent cortical parcellation technique (Amunts et al. 2000; Schleicher et al. 2000; Caspers et al. 2013). Procedures are described in detail in prior publications (Caspers et al. 2013; Lorenz et al. 2015). In brief, gray-level indices (GLIs) were determined in digitized histological sections as a measure of the volume proportion between cell bodies and the neuropil. GLI profiles were calculated along curvilinear trajectories oriented perpendicular to the cortical layers, thus measuring the GLI from Layer I/Layer II border to the innermost layer in cortical regions of interest. The shape of GLI profiles was determined based on 10 features: the mean GLI value, the position of the center of gravity on the profile curve (cortical depth), the standard deviation of the mean GLI (indicating the variability of the GLI throughout all layers), skewness and kurtosis of the profile curve, and the respective features from the profile's first derivative (Amunts et al. 2000; Schleicher et al. 2000). The borders between areas were determined based on the cortical position of the greatest difference between neighboring GLI profiles quantified by the Mahalanobis distance and tested for significance (Hotelling's T^2 test; Bonferroni-corrected). Areal borders are expected at positions along the cortical ribbon showing a significant dissimilarity in laminar patterns between adjacent blocks of profiles. To assure that the areal boundary was not dependent on the block size, the procedure was titrated for block sizes ranging from 8 to 24 profiles per block. Cortical borders were confirmed if they were consistently positioned in adjacent histological sections and across several block sizes.

As illustrated in Figure 2B, these 4 FG cytoarchitectonic areas macroanatomically include both the FG and adjacent sulci: the medial cytoarchitectonic areas, FG1 and FG3, include the medial aspect of the FG and the CoS, while the lateral cytoarchitectonic areas, FG2 and FG4, include the lateral aspect of the FG and the OTS (Caspers et al. 2013; Lorenz et al. 2015).

Registering cROIs to Individual Cortical Surfaces

After cROIs were defined in the histological sections (Fig. 1A), they were aligned to the anatomical MRI of each PM's native brain volume (Fig. 1B) as described previously (Caspers et al. 2013; Lorenz et al. 2015). We also generated cortical surface reconstructions of each PM brain by manually segmenting the anatomical MRI to differentiate gray and white matter using ITK-SNAP (http://www.itksnap.org/pmwiki/pmwiki.php). From the boundary between white and gray matter, we reconstructed the cortical surfaces in both mrVista and FreeSurfer. Each individual's cROIs were then projected to their cortical surface (Fig. 1C).

Registration of Functional and Cytoarchictectonic ROIs to the Freesurfer Average Brain

To examine the correspondence between cROIs and fROIs in a common anatomical space, we used CBA implemented in FreeSurfer (http://surfer.nmr.mgh.harvard.edu) to align each subject's cortical surface and ROIs to the FreeSurfer average brain, which is an average of the cortical surface of 39 independent participants (Fischl et al. 1999). As both living and PM subjects had regions of interest defined in the mrVista software package, the alignment process for fROIs and cROIs was the same. Both cROIs and fROIs were saved as NIfTI files, imported into FreeSurfer, and projected to the respective cortical mesh of each subject in FreeSurfer. Using CBA, each subject's ROIs were aligned to the FreeSurfer average brain (Fischl et al. 1999). This CBA uses a high-dimensional nonlinear registration algorithm, which aligns the cortical folding patterns of each subject to the cortical folding patterns of the FreeSurfer average cortical surface. A mapping of the cortical folding patterns of each subject and the template to a sphere generate a point-to-point correspondence between subjects on the FreeSurfer average cortical surface.

Maximum Probability Maps of Cytoarchitectonic ROIs

On the FreeSurfer average cortical surface, we generated a maximum probability map (MPM) of each cROI using data from 10 PM brains (Fig. 3). We transformed each binary cROI (i.e., 1 where the cROI is present and 0 elsewhere) to the common cortical surface and then averaged them on the common surface to generate a probabilistic map of each ROI. The value at each node of the map indicates the proportion of subjects that overlapped at that node for a given cROI (Fig. 3A). We then used an exhaustive, leave-one-out cross-validation procedure to determine the threshold that produced the most predictive probabilistic cROIs (Fig. 3B). We estimated the predictability of the probabilistic cROIs by calculating the dice coefficient between the left-out and predicted cROIs: Dice Coefficient = $\frac{2\,|P \cap A|}{|P| + |A|}$, where P are the nodes of the probabilistic cROI and A are the nodes of the actual cROI of the left-out subject. Since our cROIs are neighboring, probabilistic cROIs can have shared nodes on the FreeSurfer average cortical surface. Thus, to ensure that each node in the common cortical surface is assigned to a single cROI, we generated an MPM of each probabilistic cROI. The MPMs were

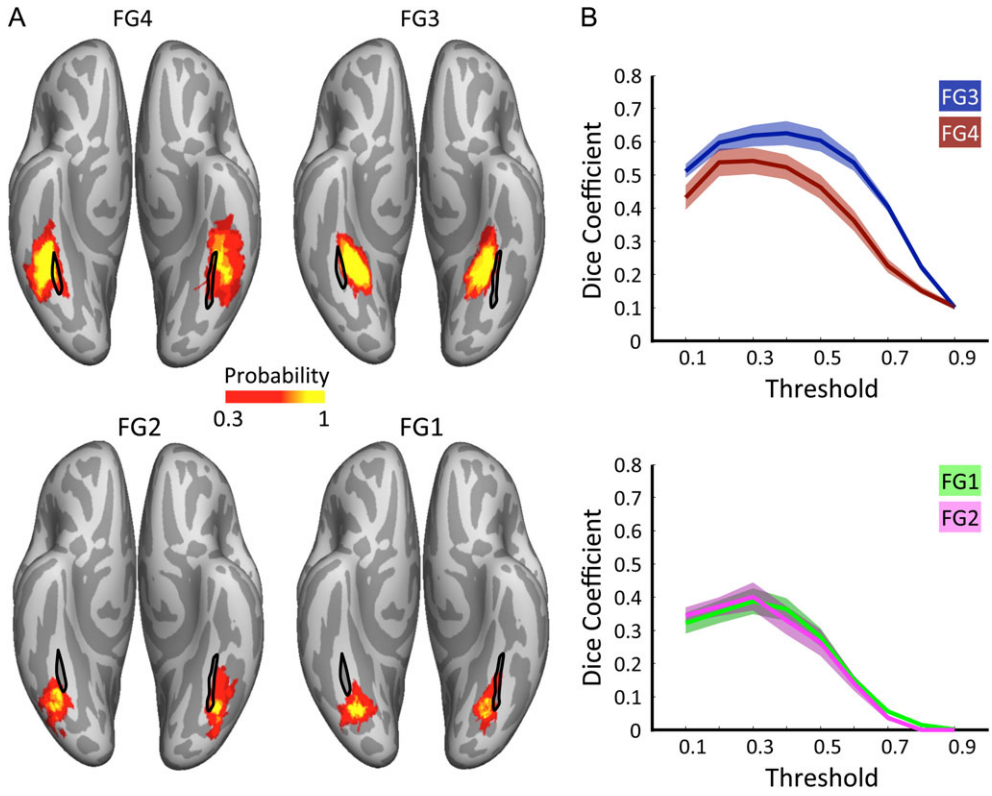

Figure 3. Cross-validated probabilistic maps of cytoarchitectonic areas. (*A*) Probabilistic maps of cytoarchitectonic areas on the Freesurfer (FS) average cortical surface. Colors indicate the proportion of overlapping subjects at each point on the cortical surface. *Black outline:* mid-fusiform sulcus (MFS). The arrangement of the probabilistic cROIs on the FS average cortical surface maintains the relation to the cortical folding as seen in individual subjects. Specifically, the MFS serves as the boundary between the probabilistic map of FG1 and FG2 (Weiner et al. 2014) and the boundary between probabilistic map of FG3 and FG4 (Lorenz et al. 2015). *Top:* FG4 and FG3. *Bottom:* FG2 and FG1. (*B*) Exhaustive, leave-one-out cross-validation of group probability maps for each cROI. Each map was generated with 9 subjects. Then, we evaluated how well this map predicted the left-out subject using the dice coefficient. This process was done 10 times for each left-out subject. Across FG1–FG4, the best dice coefficient was obtained at thresholds of 0.3–0.4. Thus, for subsequent analyses, we used the 0.3 threshold. *Line:* mean dice coefficient. *Shaded area:* standard error of the mean. *Top:* FG4 and FG3. *Bottom:* FG2 and FG1. Direct comparison of the MPMs of these cROIs across hemispheres is illustrated in Supplementary Figure 1.

generated by first finding all overlapping nodes on the cortical surface among the probabilistic cROIs and then assigning those nodes to the cROI with the highest overlap across subjects. For example, if a given node on the cortical surface had a probabilistic value of 0.3 for FG1 and a probabilistic value of 0.6 for FG3, then this node was assigned to the MPM of FG3 and excluded from the MPM of FG1. We make these MPM ROIs freely available for download with FreeSurfer and also directly from this link: vpnl.stanford.edu/FGcROIAtlas.

Additionally, we also aligned the MPMs of our cROIs to the FS average_sym template (Greve et al. 2013), which is a cortical surface that enables between-hemisphere comparisons. Aligning the MPMs of our cROIs to this surface illustrates that the topological layout of each area relative to cortical folding is largely similar between the right and left hemispheres. Nevertheless, there are also slight differences. For example, FG3 and FG4 extend more anteriorly in the left compared with the right hemispheres. Additionally, FG2 extends more laterally in the right compared with the left hemisphere (Supplementary Fig. 1). Importantly, these slight topological deviations between hemispheres are also clearly evident in Figure 3.

Measuring the Correspondence between ROIs and cROIs

We quantified the correspondence between fROIs and cROIs by calculating the percentage overlap between each individual participant's fROIs and the MPM of each cROI (Figs. 4, 7). Importantly, to assess if these overlap values are meaningful, we computed the chance proportion overlap between fROIs and cROIs using permutation testing and then determined if the overlap values were significantly different than the estimated chance level. We estimated 2 kinds of chance overlap proportions: 1) the chance proportion overlap between a given fROI and any of the cROIs and 2) the chance proportion overlap between any of the fROIs and any of the cROIs. The former was done by randomly choosing cROIs and calculating the overlap between a given fROI and a randomly chosen cROI, and the latter was done by randomly choosing both fROIs and cROIs. Permutations were done with 400 iterations per fROI per hemisphere and 400 iterations per cROI per hemisphere. Figures 4 and 7 show the latter estimate of chance overlap. While there were numerical differences across methods, the range of chance overlap from both methods was similar ranging between 0.2 ± 0.03 and 0.25 ± 0.03.

Finally, we examined the spatial relationship between fROIs and cROIs in each participant. Using CBA, we projected the MPM of each cROI to the individual surface of each individual living participant (Fig. 1*E*). This enabled us to 1) visualize the correspondence between the MPM of the cROI and each participant's fROIs and 2) examine the pattern of errors when fROIs were not perfectly aligned to cROIs (4 example participants are shown in Fig. 8).

In addition to our single-subject analyses, we also generated MPMs of fROIs on the FreeSurfer average cortical surface using

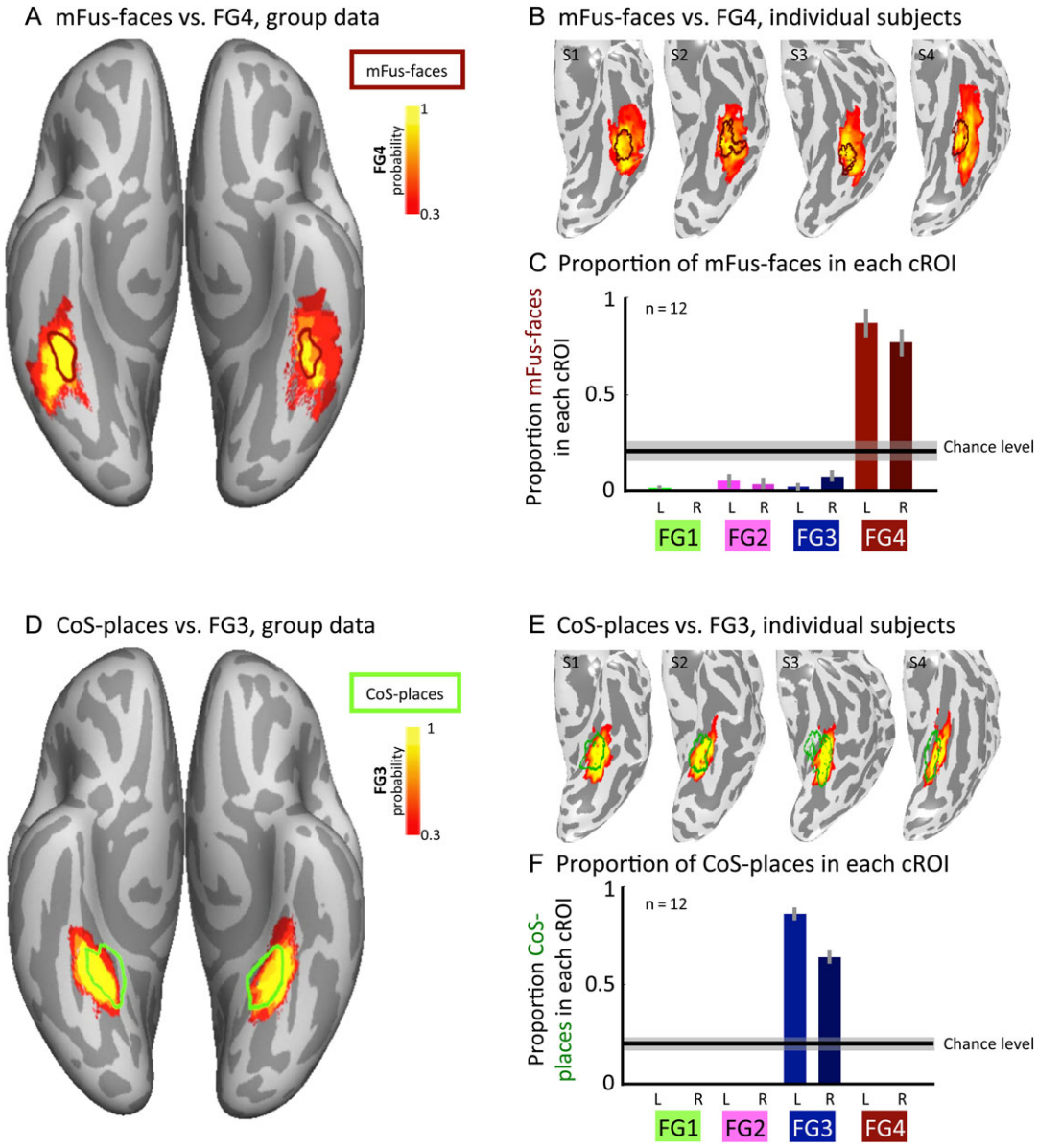

Figure 4. Face- and place-selective regions are located in distinct cytoarchitectonic areas. (*A*) Dark red outline of the MPM for mFus-faces/FFA-2 from 12 living individuals superimposed on the MPM for FG4 from 10 PM brains. (*B*) Four example left hemispheres illustrating mFus-faces/FFA-2 in individual subjects relative to the MPM of FG4. (*C*) Mean proportion overlap of mFus-faces/FFA-2 relative to each cROI. *Errorbars:* Standard error of the mean across 12 subjects. *Horizontal bar:* chance overlap probability. (*D* and *E*) Same as A and B, but for CoS-places/PPA (green outline) and FG3. (*F*) Same as (*C*), but for CoS-places/PPA.

data from all living participants using the same method as described above for cROIs. We then registered MPMs of all functional regions and cytoarchitectonic areas to the FreeSurfer average cortical surface to generate a group-level summary of functional–cytoarchitectonic relationships in human VTC (Fig. 9).

It should also be stated that we cannot rule out the possibility that there are slight imprecisions in our approach because of individual subject variability in fROIs, patterns of cortical folding, and their relationship. However, we are confident in the accuracy of our approach as the resulting group MPMs of fROIs and cROIs accurately preserve the topology of each type of ROI and cortical folding in individual subjects, which indicates the precision of these alignment techniques as previously shown (Fischl et al. 2008; Hinds et al. 2009). Errors exist in any study directly comparing living and PM brains and are unavoidable until there will be new methods that will enable measuring cytoarchitectonic areas in vivo, which will, in turn, allow the direct comparison between cROIs and fROIs within the same individuals.

Examining the Effect of Contrast on the Distribution of Category Selectivity Values within Each cROI

To complement the analyses described above examining the coupling between fROIs and cROIs, we also assessed the functional–cytoarchitectonic relationship within VTC by comparing the distribution of category selectivity values across all voxels within each cROI. This analysis is hypothesis-free as it 1) does not necessitate localizing any fROIs and 2) is not dependent on the threshold or contrast used to define fROIs. To perform this analysis, each probabilistic cROI was transformed to each living

participant's brain. Selectivity in each voxel within each cROI was then determined by the *t*-value of the GLM contrast. In Figure 5, we illustrate the distribution of face- and place-selectivity across all voxels of FG3 and FG4. We assessed selectivity to faces in each voxel using 2 contrasts: 1) preferred versus other categories and 2) preferred versus places. Selectivity to places in each voxel was assessed with 2 contrasts: 1) places versus other categories and 2) places versus faces. We conducted a non-parametric Kolmogorov–Smirnov test (K-S test) to determine if the distributions of selectivity values in FG3 and FG4 were significantly different from each other in each subject. Additionally, we include distributions of selectivity values for all categories and all FG cROIs in Supplementary Figures 2–5. Finally, to test if category selectivity significantly differed across cROIs, we ran a 3-way analysis of variance (ANOVA) on the mean selectivity using category, hemisphere, and cROI as factors.

Transforming MPMs of Face- and Place-Selective fROIs to Histological Sections

Using CBA, we registered the MPM of face-selective and place-selective fROIs to the cortical surface of each PM brain. From the PM's cortical surface, we registered both of these MPMs to the original PM brain volume obtained with an MRI scan. Then, we registered these MPM fROIs to the reconstructed 3D histological volume using a nonlinear transformation implemented in ANTS (https://sourceforge.net/projects/advants/). Code used for this transformation can be found here: github.com/VPNL/cyto-functional. This procedure localizes the MPM fROIs to the original histological slices within which the FG cROIs were defined, consequently enabling the extraction of GLI profiles from the probabilistic location of each fROI in histological sections (Fig. 6).

In these analyses, we focused on face- and place-selective regions because they are located centimeters away from each other across the cortical ribbon and are identifiable on single histological sections with distinct macroanatomical landmarks. As such, we were able to validate the accuracy of the localization of fROIs in histological sections using 2 distinct domain-specific macroanatomical landmarks: 1) the MFS as a landmark for mFus-faces/FFA-2 (Weiner et al. 2014) and 2) the branching of the CoS and intersection with the nearby anterior lingual sulcus as landmarks for the anterior portion of CoS-places/PPA (Weiner et al. Under review).

Results

Are Face- and Place-Selective Regions Cytoarchitectonically Dissociable?

We first assessed the correspondence between the cortical location of cytoarchitectonic areas within VTC relative to face-selective (mFus-faces/FFA-2) and place-selective (CoS-places/PPA) regions as these are 2 of the most widely studied domain-specific regions in VTC, and their arrangement relative to the cortical folding is consistent across individuals. Qualitative assessments of the cortical location of mFus-faces/FFA-2 and CoS-places/PPA relative to cytoarchitectonic areas indicate that each of these regions is located within distinct cytoarchitectonic areas. At the group level, mFus-faces/FFA-2 is located within FG4 (Fig. 4A) and CoS-places/PPA is located within FG3 (Fig. 4D). Quantitative evaluation of the overlap between fROIs in individual participants and the probabilistic maps of each of the 4 FG cROIs revealed that 81 ± 24% (mean ± standard deviation) of mFus-faces/FFA-2 is located within FG4 (Fig. 4C) and

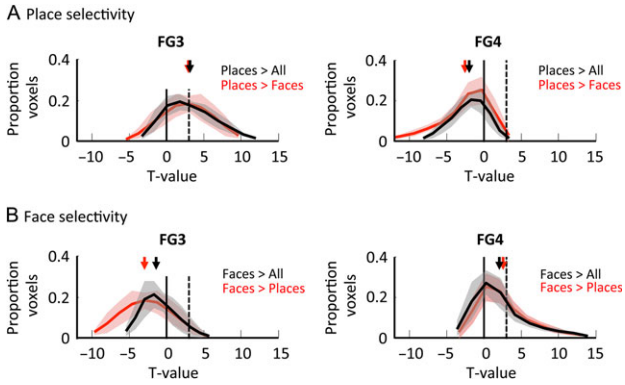

Figure 5. Place-selective voxels are localized to FG3 and face-selective voxels are localized to FG4. (*A*) Distribution of place-selectivity across all voxels of cytoarchitectonic areas FG3 (left) and FG4 (right) for 2 contrasts: places versus all other categories (black) and places versus faces (red). For both contrasts, FG3 illustrates a distribution with an average positive selectivity for places, while FG4 illustrates a distribution with an average negative selectivity for places. (*B*) Distribution of face-selectivity across all voxels of cytoarchitectonic areas FG3 (left) and FG4 (right) for 2 contrasts: faces versus all other categories (black), and faces versus places (red). For both contrasts, FG3 illustrates a distribution with an average negative selectivity for faces, while FG4 illustrates a distribution with an average positive selectivity for faces. *Shaded areas:* standard deviation across 12 subjects. *Arrows:* average selectivity. *Dashed vertical line:* threshold used to define fROIs ($t = 3$). *Solid vertical line:* $t = 0$.

75 ± 11% of CoS-places/PPA is located within FG3 (Fig. 4F). These levels of overlap are significantly above chance (*t*s > 8.5, *P*s < 10^{-8}, Fig. 4C,F-horizontal line) and show a significant fROI by cROI interaction ($F(3,88) = 380$, $P < 10^{-6}$, 2-way ANOVA with factors of fROI and cROI). Visualizing the location of fROIs relative to cROIs in each participant (Fig. 4B,E) shows that the relationship among fROIs and cROIs is visible at the individual subject level: mFus-faces/FFA-2 is located within FG4 and rarely extends medially from FG4 into FG3 (Fig. 4B,C), while CoS-places/PPA is largely located within FG3. Note that portions of CoS-places/PPA not in FG3 extend medially into the lip of the CoS and the parahippocampal gyrus and rarely deviate into FG1, FG2, or FG4 (Fig. 4E,F). Thus, mFus-faces/FFA-2 and CoS-places/PPA are located within different cytoarchitectonic areas.

We complemented these analyses by comparing the distribution of face- and place-selectivity values in FG3 and FG4. This analysis is hypothesis-free because it does not require the definition of fROIs. Results show that while the contrast quantitatively affects selectivity values, it does not qualitatively change the pattern of results. Specifically, independent of contrast, FG3 and FG4 are differentially selective for places and faces, respectively (Fig. 5; 2-sample K-S tests comparing the distributions of selectivity in FG3 and FG4 for all 4 contrasts: all K-S stats > 0.3, all *P*s < 10^{-6}). Likewise, a 4-way ANOVA of mean selectivity using as factors cROI (FG3/FG4), preferred category (faces/places), contrast (preferred versus the other category/preferred versus all categories), and hemisphere, reveals a significant cROI x preferred category interaction ($F(3,352) = 348.51$, $P < 10^{-6}$), as well as significant cROI × preferred category × contrast interaction ($F(3,352) = 5.12$, $P < 0.002$). The former interaction indicates that changing the contrast does not qualitatively affect the result that FG3 and FG4 exhibit different category preferences, while the latter (weaker) interaction reflects that changing the contrast quantitatively affects the magnitude of the *t*-values. These results complement our prior analyses and provide empirical support demonstrating that the

coupling between face-selectivity and FG4, as well as place-selectivity and FG3, generalizes across analyses and is not dependent on the definition of fROIs.

What Are the Cytoarchitectonic Features of Face- and Place-Selective Regions?

We probed the underlying cytoarchitecture of mFus-faces/FFA-2 and CoS-places/PPA directly by back-projecting the MPMs of these functional regions to cell body–stained sections and then extracting histological profiles of these regions to examine the distribution of cells across layers (Fig. 6). This is akin to functional ROI analyses in which an ROI is localized with one set of data, and functional properties are determined from independent data. For the first time, instead of probing functional properties of a region, we extract cytoarchitectonic properties to reveal the cellular structure of regions selective for faces and places.

Results show that mFus-faces/FFA-2 and CoS-places/PPA have distinct cytoarchitectonic features as represented by GLI profiles of cell body density across layers. The GLI profile of mFus-faces/FFA-2 is characterized by a prominent sublayer IIIc with medium- to large-sized pyramidal cells, a moderately dense layer IV, and a slight overall increase of GLI from layer II to layer VI with several local maxima and minima, but an absolute maximum in layer VI (Fig. 6C–E). By contrast, CoS-places/PPA is characterized by a relatively compact, dense layer II, a layer IV with little clusters of granular cells, and a GLI curve that does not show a trend to increase towards layer VI as found in mFus-faces/FFA-2 (Fig. 6C–E). These results reveal the cytoarchitectonic features of face- and place-selective regions for the first time and show that these regions have distinct cytoarchitectonic characteristics.

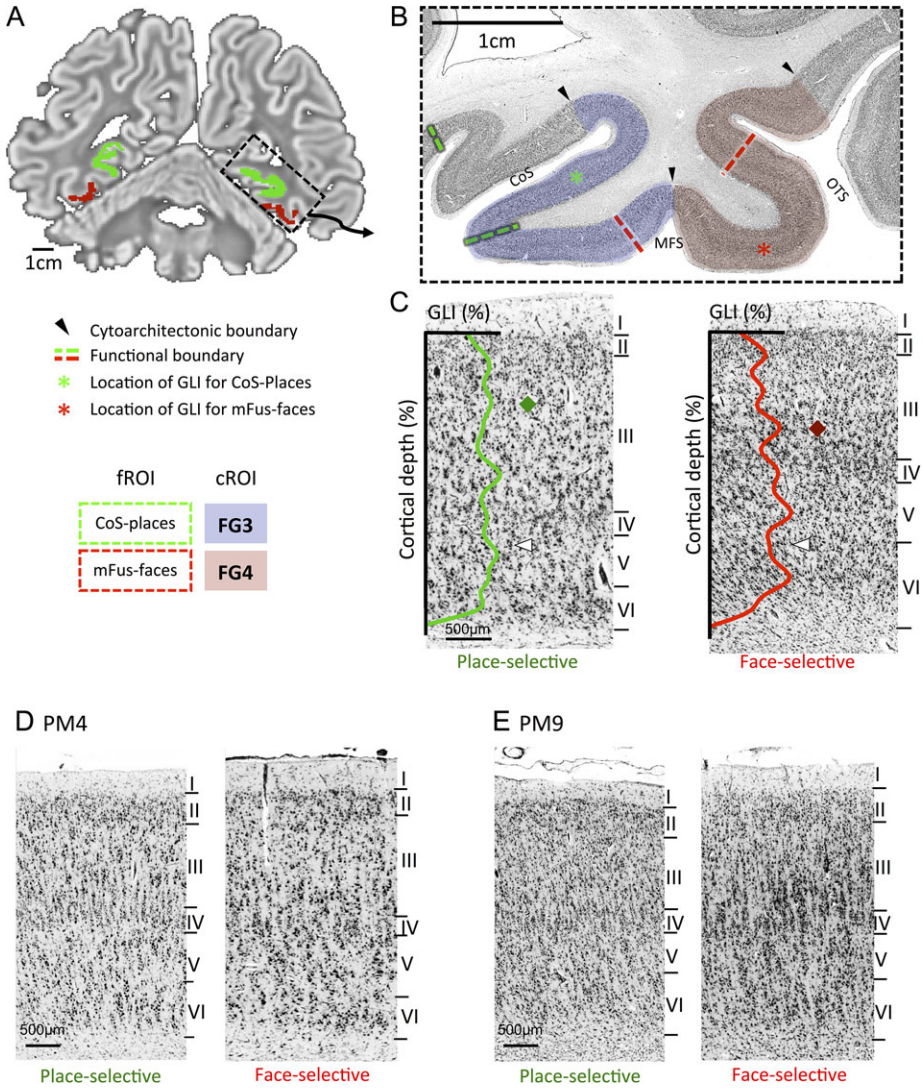

Figure 6. Cytoarchitectonic profiles of face- and place-selective regions. (*A*) MPM of mFus-faces/FFA-2 (red) and CoS-places/PPA (green) projected onto a reconstruction of a histological slice from an example PM brain. (*B*) Zoomed view of the cell body–stained histological section within the rectangular region shown in (*A*). *Arrows:* boundaries of cROIs; *Dashed lines:* boundaries of CoS-places/PPA (green) and mFus-faces/FFA-2 (red). (*C*) Example histological slices and corresponding GLI profiles within CoS-places/PPA and mFus-faces/FFA-2 from the locations indicated by the green and red asterisks in (*B*), respectively. *Green and red curves*: GLI of cell density across layers. Note differences in cell density, laminar structure, and cell body size between the 2 sections. *White arrowheads:* different cell density as estimated by the GLI in V/VI, illustrating heterogeneously packed layers V/VI of FG4 compared with the more homogeneous layers V/VI of FG3. *Diamonds:* broad and cell-sparse layers IIIa/b of FG3 versus prominent and broad layer IIIc of FG4. (*A–C*) Data from PM1. (*D* and *E*) Example cytoarchitectonic profiles within CoS-places/PPA and mFus-faces/FFA-2 from 2 additional PM brains. (*D*) PM4. (*E*) PM9.

Regions Selective for the Same Domain are Cytoarchitectonically Dissociable

As there are multiple face-selective regions in bilateral VTC (Weiner and Grill-Spector 2010; Fig. 2A), we tested if regions selective for the same domain are cytoarchitectonically dissociable or not. Finding that regions selective for the same domain are located within different cytoarchitectonic territories would provide empirical evidence supporting that these regions should be separated based on different cellular features. However, finding that regions selective for the same domain are located within the same cytoarchitectonic territory would provide evidence suggesting a common neural hardware that is optimized to process stimuli of that domain, and furthermore, that it is adequate to combine these functional regions.

Our data reveal that functional regions selective for the same domain are cytoarchitectonically dissociable. Specifically, functional regions that are situated anatomically posterior in lateral VTC are cytoarchitectonically distinct from those that are situated anatomically more anterior. In the domain of face-selectivity, mFus-faces/FFA-2 is located largely in FG4, while pFus-faces/FFA-1 is located largely within FG2 (Figs 7A and 8E, significant fROI by cROI interaction, $F(3,88) = 53.4$, $P < 10^{-6}$, 2-way ANOVA with factors of fROI and cROI). As FG2 and FG4 illustrate cytoarchitectonic differences—for example, FG2 has a conspicuous layer III with larger pyramidal cells than those in FG4, as well as a prominent and dense layer IV compared with FG4, which has a thin and moderately dense layer IV—these results suggest a different cellular architecture in pFus-faces/FFA-1 compared with mFus-faces/FFA-2.

In the domain of reading, there are also multiple character-selective regions in lateral VTC of the left hemisphere (Stigliani et al. 2015; Fig. 2A). Similar to our findings with respect to the organization of face-selective regions, the more anterior mOTS-chars/VWFA-2 is located within FG4 (Fig. 7B, Fig. 8D), while the more posterior pOTS-chars/VWFA-1 is largely located within FG2 (significant fROI by cROI interaction $F(3,80) = 32$, $P < 10^{-6}$, left hemisphere, Figs 7B and 8F). Together, these data indicate that functional regions that are selective for the same domain in posterior and mid portions of lateral VTC, respectively, are located in different cytoarchitectonic territories.

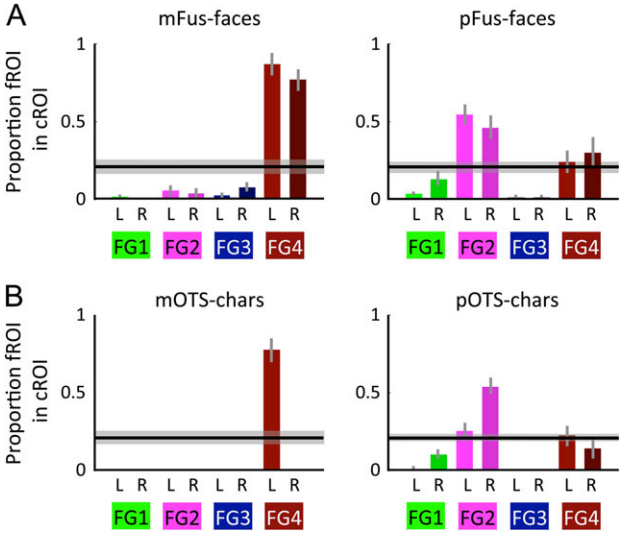

Figure 7. Cytoarchitectonic segregation within-domain in lateral VTC. Each panel shows the mean proportion overlap of each fROI relative to each of the 4 FG cROIs. Data are averaged across 12 subjects. (A) Face-selective regions. The more posterior pFus-faces/FFA-1 is cytoarchitectonically distinct from the more anterior mFus-faces/FFA-2. (B) Character-selective regions. The more posterior pOTS-chars/VWFA-1 is cytoarchitectonically distinct from the more anterior mOTS-chars/VWFA-2. *Errorbars*: between-subject SEM.

There is a Many-to-One Mapping between Functional Regions and Single Cytoarchitectonic Areas in Human VTC

The prior analyses not only indicate that regions selective for the same domain are cytoarchitectonically dissociable but also suggest that multiple fROIs are contained within a single cROI. Furthermore, as the surface areas of FG4 (957 ± 109 mm^2) and FG2 (619 ± 75 mm^2), respectively, are 2–3 times larger than that of face- (268 ± 32 mm^2) or character-selective regions (268 ± 32 mm^2), it is likely that there is a many-to-one mapping between multiple functional regions and single cytoarchitectonic areas in human VTC. Indeed, quantifying this correspondence reveals that FG4 contains 3 functional regions selective for different domains: 1) 81% ± 24% of mFus-faces/FFA-2; 2) 79 ± 25% of OTS-bodies/FBA, and 3) 77 ± 25% mOTS-chars/VWFA-2 (Figs 7, 8B–D). This many-to-one mapping between multiple fROIs and a single cROI is also observed in the posterior FG, albeit more weakly: 49.5 ± 24% of pFus-faces/FFA-1 and 40 ± 18% of pOTS-chars/VWFA-1 are both located within FG2 (Figs. 7, 8E–F). Additionally, there are hemispheric differences: a larger portion of pOTS-chars/VWFA-1 overlaps FG2 in the right than left hemisphere, and the opposite is observed for pFus-faces/FFA-1 (3-way fROI × cROI × hemisphere interaction, $F(3,176) = 4.5$, $P \leq 0.005$).

We also examined the distribution of selectivity across voxels for all categories and cROIs as we did for face-selectivity and place-selectivity in FG3 and FG4. Results replicate the fROI-cROI comparison, where voxels with substantial character selectivity are largely located in FG2 and FG4, but not FG1 and FG3 (Supplementary Fig. 4). Body-selective voxels were located in FG4 but not FG1 and FG3 (Supplementary Fig. 5). Additionally, while none of our fROIs overlapped with FG1, this analysis revealed that FG1 showed weak, but positive place-selectivity (Supplementary Fig. 2), which is consistent with recent findings of weak place-selectivity posterior to the more anterior CoS-places/PPA (Baldassano et al. 2013; Silson et al. 2015). Finally, a 3-way ANOVA on the mean selectivity of each of the 4 cROIs for faces, places, characters, and bodies using cROI, category, and hemisphere as factors found a strong and significant interaction between cROI and category ($F(9,736) = 146.3$, $P < 10^{-6}$), as well as a weak but significant interaction between cROI, category, and hemisphere ($F(9,736) = 2.9$, $P < 0.002$). Together, these analyses indicate differential functional characteristics across cROIs, as well as illustrate that our results are not analysis-specific or dependent on the definition of fROIs.

Summary of Functional and Cytoarchitectonic Organization of Human VTC

To provide a complete group-level summary of the relationship between the cytoarchitectonic and functional organization of human VTC, we generated an overlay of the MPMs of the 6 fROIs selective to faces, bodies, characters, and places relative to the MPM of the 4 FG cROIs (Fig. 9). The group-level visualization mirrors the organization quantified at the individual subject level. In summary, 1) CoS-places/PPA is largely in FG3, 2) mFus-faces/FFA-2, OTS-bodies/FBA, and mOTS-chars/VWFA-2 are within FG4, and 3) pFus-faces/FFA-1 and pOTS-chars/VWFA-1 are largely within FG2. Altogether, these results suggest that

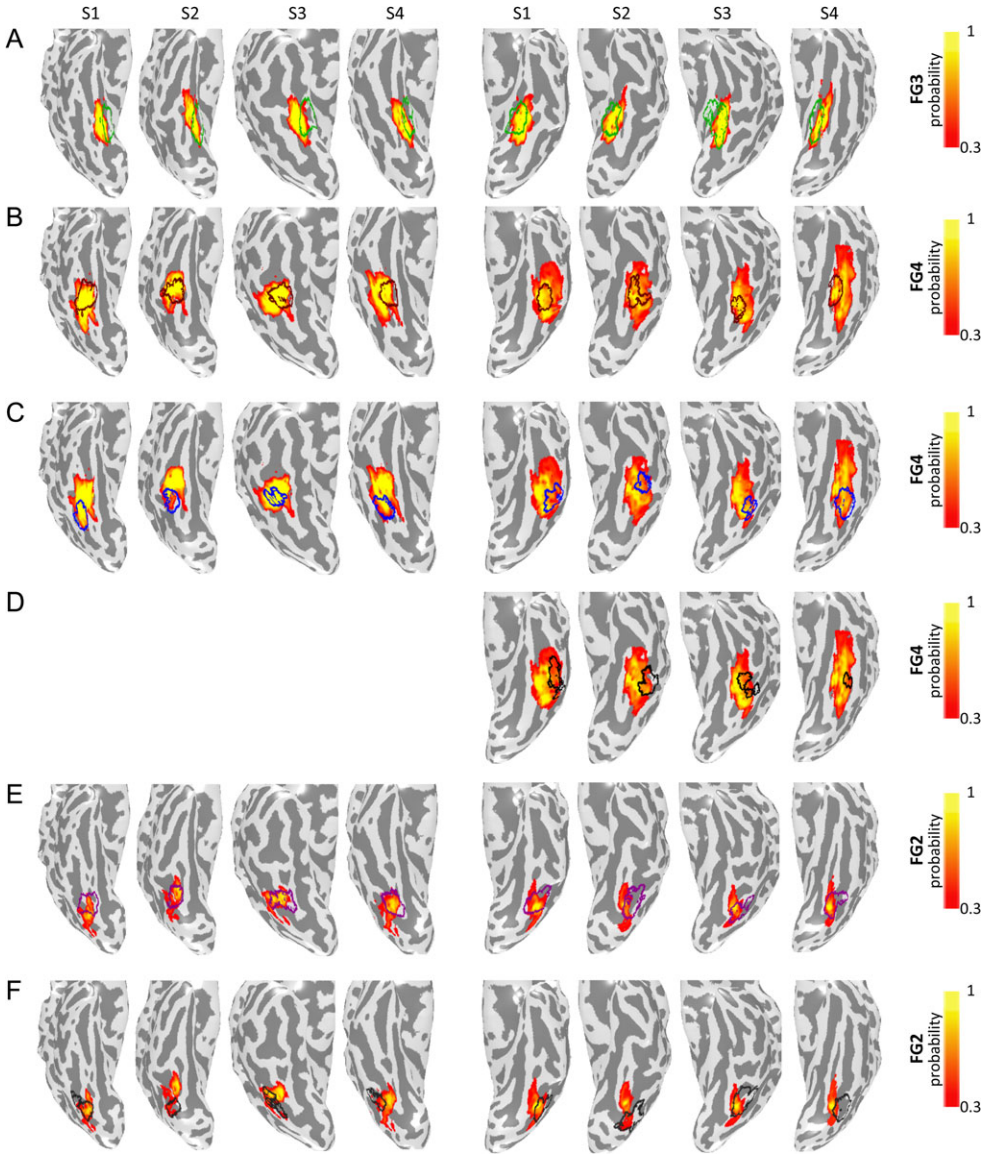

Figure 8. The functional and cytoarchitectonic organization of human VTC in individual subjects. Each panel shows the spatial relation of an fROI (contour) and a maximum probability cROI (indicated by the color map on the right) in an example hemisphere. Data are shown on the native inflated cortical surface of each subject. The same 4 example subjects are shown in all panels. *4 left panels:* right hemisphere; *4 right panels:* left hemisphere. (*A*) CoS-places/PPA and probability map of FG3; Left hemispheres are same as Figure 4*E*. (*B*) mFus-faces/FFA-2 and probability map of FG4. Left hemispheres are same as Figure 4*B*. (*C*) OTS-bodies/FBA and probability map of FG4. (*D*) mOTS-chars/VWFA-2 and probability map of FG4. (*E*) pFus-faces/FFA-1 and probability map of FG2. (*F*) pOTS-chars/VWFA-1 and probability map of FG2.

cytoarchitecture contributes to functional segregation both within and across domains, but there are also cytoarchitectonic similarities among regions selective for different domains especially within area FG4.

Discussion

By leveraging recent advancements in understanding the functional and cytoarchitectonic organization of human VTC, we were able to link functional regions in living participants to cytoarchitectonic areas in PM histological slices within VTC for the first time. Our findings provide empirical evidence supporting the hypothesis that cellular features contribute to functional organization in human VTC. The finding of a many-to-one mapping between domain-specific regions and a single cytoarchitectonic area in human VTC challenges classic theories in the field of neuroscience proposing that there is a one-to-one mapping between functional and cytoarchitectonic areas (Campbell 1905; Smith 1907; Brodmann 1909). We discuss the implications and theoretical ramifications of our findings in the subsequent sections.

Beyond BOLD: Linking Cellular Architecture to the Functional Organization of Domain-specific Regions

These findings provide the first insight into the cellular architecture of domain-specific regions in human VTC. This is an important advancement for 3 reasons. First, previous fMRI studies have shown that the functional organization of high-level visual regions in the FG and surrounding cortex is reproducible across individuals (Levy et al. 2001; Nasr et al. 2011; Julian et al. 2012;

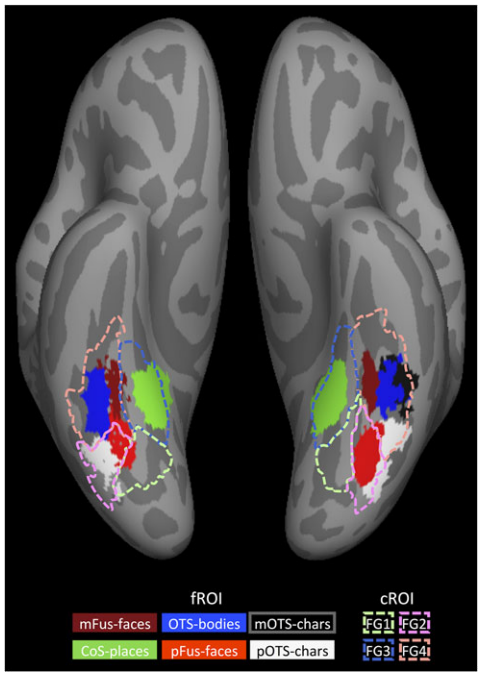

Figure 9. Cytoarchitectonic segregation within-domain and cytoarchitectonic integration across domains. A summary of the relationship between cROIs (contours) and fROIs (solid) in human VTC. MPMs of the cROIs and fROIs are displayed on the FreeSurfer average cortical surface.

Weiner et al. 2014). The findings from the present study show that these measurements from a blood oxygen–dependent signal, which is an indirect measure of neural activity, have cellular underpinnings. Second, fMRI measurements are at a larger spatial scale than the cortical microstructure. As such, we have improved our scale of understanding regarding the functional–structural organization of human VTC from centimeters to microns. Third, we provide new insights regarding the functional–cytoarchitectonic organization of the FG, which cannot be inferred from prior research in non-human primate inferotemporal cortex (Gross et al. 1972; Van Essen and Zeki 1978; Boussaoud et al. 1991; Zangenehpour and Chaudhuri 2005; Borra et al. 2010) because the FG is a hominoid-specific structure absent in the macaque brain (Nasr et al. 2011; Weiner and Zilles 2016).

This study provides the first evidence that cellular differences contribute to functional segregation of domain-specific regions in human high-level visual cortex. This segregation on the cortical sheet occurs for regions selective for different domains as well as for distinct regions processing information from the same domain. Specifically, we find that differences in cellular architecture distinguish 1) human face- and place-selective regions and 2) regions selective for the same domain even if they are located on the same macroanatomical territory, such as face-selective regions on the FG. Regarding the latter finding, our results show that defining one large face-selective region on the FG—perhaps due to a less stringent contrast (e.g., faces > places) and/or a weak statistical threshold (e.g., $t > 2$)—as a single area (e.g., the FFA) would result in a functional region consisting of 2 distinct cytoarchitectonic components. As cytoarchitectonic differences are used to parcellate brain areas (Campbell 1905; Smith 1907; Brodmann 1909; Hubel and Wiesel 1977; Van Essen 2003), these findings provide strong, microanatomical evidence to separate these functional regions in human VTC.

Notably, we also find evidence for cytoarchitectonic similarities among regions processing information from different domains. Specifically, 1) cytoarchitectonically defined area FG4 contains 3 different domain-specific regions selective for faces, bodies, and characters and 2) cytoarchitectonically defined FG2 contains 2 different domain-specific regions selective for faces and characters. This finding of a common cellular architecture among regions processing stimuli from different domains suggests the possibility that these functional regions share a common computational need that is implemented by a common cytoarchitecture (we discuss this hypothesis in detail in the next section). Alternatively, while the cytoarchitecture of different domain-specific regions (e.g., for faces and characters) may be common, there may be differences in other micron-level features, such as connectivity among neurons (Reckfort et al. 2015) and/or receptor architectonics (Caspers et al. 2015), which are undetected by the present method and may give rise to specialized neural circuitry for processing stimuli of particular domains. These possibilities can be tested in future research.

We recognize that a limitation of the present study is that individual fROIs are compared to probabilistic locations of cROIs and probabilistic fROIs are compared to individual cROIs. Nevertheless, currently there is no method that enables cytoarchitectonic analyses *in vivo*. Further, prior studies relating cROIs and fROIs in human VTC were conducted at the group level (Van Essen et al. 2012; Abdollahi et al. 2014; Caspers et al. 2014). Thus, our approach quantifying the correspondence between MPM cROIs and fROIs in individual participants, and back-projecting MPM fROIs to individual 3D-reconstructed histological sections provides the most accurate method to date relating the functional and cytoarchitectonic organization of human VTC.

A New Hypothesis: Two Computational Axes in Human VTC

These findings illustrate that cytoarchitectonic and functional organizational features of human VTC correspond to 2 dimensions on the cortical sheet (Fig. 10). The first is a lateral–medial axis that differentiates regions across domains. The second is an anterior–posterior axis that distinguishes regions within a domain.

We propose that the lateral–medial axis is an axis of specialization (Grill-Spector and Malach 2004). The physical segregation of regions from different domains may enable efficient parallel processing of domain-specific information either 1) within separate cytoarchitectonic areas (e.g., face information in FG4 and place information in FG3) or 2) within the same cytoarchitectonic area (e.g., character, body, and face information on a lateral–medial gradient within FG4). The former supports the theory that domain-specific regions that are cytoarchitectonically distinct perform different computations. The latter suggests a new theory that domain-specific regions can be cytoarchitectonically similar and consequently computationally related. For example, throughout the visual system, anatomical properties of cells coding foveal stimuli differ from those coding peripheral stimuli (Kennedy et al. 1986; Curcio and Allen 1990; Dacey and Petersen 1992). Evidence indicates that this segregation perpetuates into high-level regions: CoS-places/PPA associated with FG3 shows a peripheral bias (Levy et al. 2001), while face- (Kay et al. 2015), word- (Hasson et al. 2002), and body-selective (Weiner and Grill-Spector 2011) regions associated with FG4 show a foveal bias. Thus, the cytoarchitectonic differences separating face- from place-selective regions may reflect different anatomical substrates supporting foveal and peripheral computations, respectively,

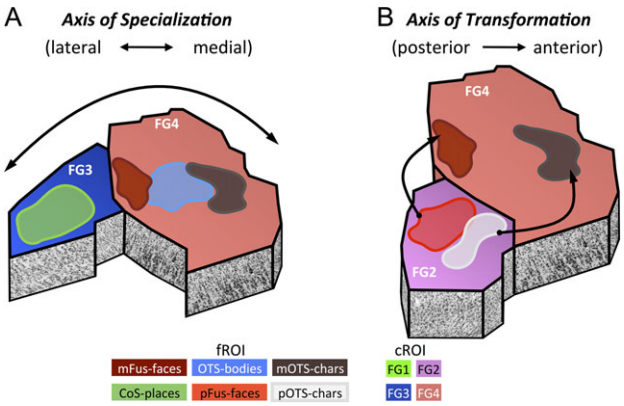

Figure 10. Two computational axes in VTC. A schematic illustration of the 2 proposed computational axes in VTC. (*A*) The lateral–medial axis is an axis of specialization both within and across cytoarchitectonic areas. FG3 and FG4 are depicted relative to domain-specific regions to illustrate the proposed lateral–medial axis of specialization. (*B*) The posterior–anterior axis is an axis of transformation. FG2 and FG4 are depicted relative to face- and character-selective regions to illustrate the proposed anterior–posterior axis of hierarchical transformation within regions selective for the same domain.

while the cytoarchitectonic similarities shared between face-, body-, and character-selective regions in FG4 may reflect similar anatomical substrates supporting foveal computations. Cytoarchitectonic differences between lateral and medial VTC may underlie additional computational differences that have been observed along a lateral–medial axis in VTC (Grill-Spector and Weiner 2014) including (but not limited to) differences in temporal dynamics (Gilaie-Dotan et al. 2008) adaptation properties (Weiner et al. 2010) as well as preferences to rectilinear versus curvilinear visual features (Nasr et al. 2014).

We also propose that the anterior–posterior axis is associated with computational transformations (Grill-Spector and Malach 2004), which enable a behaviorally relevant representation to be achieved through a series of sequential computations across a cortical hierarchy (DiCarlo and Cox 2007). A hallmark of hierarchical processing is a progressive increase in population receptive field size (pRF; Wandell and Winawer 2015). Accumulating evidence suggests that face-selective regions constitute a functional hierarchy (Kravitz et al. 2013; Kay et al. 2015; Silson et al. 2015), whereby pRFs become progressively larger and more foveal (Kay et al. 2015). Therefore, we postulate that differences in cytoarchitectonics along the anterior–posterior axis reflect computational transformations linked to pRFs: regions within the same cytoarchitectonic area may have similar pRF properties irrespective of domain (e.g., mFus-faces/FFA-2 and mOTS-chars/VWFA-2), while regions located in separate cytoarchitectonic areas may have different pRF properties within-domain (e.g., pFus-faces/FFA-1 and mFus-faces/FFA-2). In this model, the different histological properties reflected along the posterior–anterior hierarchical axis reflect dedicated microanatomical hardware optimized for particular computational transformations such as position and size, which can be tested in future research.

Conclusion

These discoveries link the organization of domain-specific functional regions to the cellular heterogeneity of human VTC. Our findings integrate macroscopic functional properties and microscopic anatomical properties and show that functional and cytoarchitectonic organizational features vary along 2 cortical axes, which may reflect 2 computational axes within high-level visual cortex.

Supplementary Material

Supplementary data are available at *Cerebral Cortex* online.

Funding

Support for this research was provided by grants: 1RO1EY 02231801A1 and 1R01EY02391501A1 to K.G.S.; the European Union Seventh Framework Programme (FP7/2007–2013) under grant agreement no. 604102 (Human Brain Project) to K.A. and K.Z.; and the following grants to B.F.: the National Institute for Biomedical Imaging and Bioengineering (P41EB015896, R01EB006758, R21EB0 18907, R01EB019956), the National Institute on Aging (5R01AG00 8122, R01AG016495), the National Institute for Neurological Disorders and Stroke (R01NS0525851, R21NS072652, R01NS070963, R0 1NS083534, 5U01NS086625), and was made possible by the resources provided by Shared Instrumentation Grants 1S10RR0 23401, 1S10RR019307, and 1S10RR023043. Additional support was provided by the NIH Blueprint for Neuroscience Research (5U0 1-MH093765), part of the multi-institutional Human Connectome Project.

Author Contributions

K.S.W.: Designed the experiment, developed the pipeline and code to analyze the relationship between cytoarchitectonic and functional data, analyzed the relationship between cytoarchitectonic and functional data, and wrote the manuscript.

M.B.: Developed the pipeline and code to analyze the relationship between cytoarchitectonic and functional data, wrote code that implements the transformations between data types, analyzed the data, and wrote the manuscript.

S.L.: Defined cytoarchitectonic areas FG3 and FG4 in PM brains.

J.C.: Defined cytoarchitectonic areas FG1 and FG2 in PM brains.

A.S.: Ran fMRI experiments in living participants, analyzed the data, and defined fROIs in living participants.

K.Z.: Collected and developed methods for observer-independent analysis of cytoarchitecture, and analyzed cytoarchitectonic data in PM brains, and contributed to the manuscript.

K.A.: Collected and developed methods for observer-independent analysis of cytoarchitecture, analyzed cytoarchitectonic data in PM brains, and contributed to the manuscript.

B.F.: Developed methods for cortex-based alignment and provided design and code support for developing the pipeline relating functional and cytoarchitectonic data.

K.G.S.: Designed the experiment, developed the pipeline and code to quantify the relationship between functional and cytoarchitectonic regions, analyzed the relationship between cytoarchitectonic and functional data, wrote the manuscript, and supported this research.

Notes

We thank Miguel R. Chuapoco, Yotam de la Zerda, and David Loftus for help with manually segmenting anatomical brain volumes of PM brains. We thank Swaroop Guntupalli for help with the analyses that incorporated functions from AFNI. In addition,

B.F. has a financial interest in CorticoMetrics, an organization whose medical pursuits focus on brain imaging and measurement technologies. *Conflict of Interest:* B.F.'s interests were reviewed and are managed by Massachusetts General Hospital and Partners HealthCare in accordance with their conflict of interest policies.

References

Abdollahi RO, Kolster H, Glasser MF, Robinson EC, Coalson TS, Dierker D, Jenkinson M, Van Essen DC, Orban GA. 2014. Correspondences between retinotopic areas and myelin maps in human visual cortex. Neuroimage. 99:509–524.

Amunts K, Malikovic A, Mohlberg H, Schormann T, Zilles K. 2000. Brodmann's areas 17 and 18 brought into stereotaxic space-where and how variable? Neuroimage. 11:66–84.

Amunts K, Zilles K. 2015. Architectonic mapping of the human brain beyond Brodmann. Neuron. 88:1086–1107.

Baldassano C, Beck DM, Fei-Fei L. 2013. Differential connectivity within the parahippocampal place area. Neuroimage. 75ŒC: 236–245.

Ben-Shachar M, Dougherty RF, Deutsch GK, Wandell BA. 2011. The development of cortical sensitivity to visual word forms. J Cogn Neurosci. 23:2387–2399.

Borra E, Ichinohe N, Sato T, Tanifuji M, Rockland KS. 2010. Cortical connections to area TE in monkey: hybrid modular and distributed organization. Cereb Cortex. 20:257–270.

Boussaoud D, Desimone R, Ungerleider LG. 1991. Visual topography of area TEO in the macaque. J Comp Neurol. 306: 554–575.

Brodmann K. 1909. The principles of comparative localisation in the cerebral. In: Cortex based on cytoarchitectonics. Lausanne, Switzerland: Springer.

Bugatus L, Weiner KS, Grill-Spector K. 2015. Task differentially modulates the spatial extent of category-selective regions across anatomical locations. J Vis. 15:1170.

Bugatus L, Weiner KS, Grill-Spector K. 2016. Differential representation of category and task information across high level visual cortex and ventro-lateral prefrontal cortex. J Vis. 16:256.

Campbell AW. 1905. Histological studies on the localisation of cerebral function. Cambridge: Cambridge University Press.

Caspers J, Palomero-Gallagher N, Caspers S, Schleicher A, Amunts K, Zilles K. 2015. Receptor architecture of visual areas in the face and word-form recognition region of the posterior fusiform gyrus. Brain Struct Funct. 220:205–219.

Caspers J, Zilles K, Amunts K, Laird AR, Fox PT, Eickhoff SB. 2014. Functional characterization and differential coactivation patterns of two cytoarchitectonic visual areas on the human posterior fusiform gyrus. Hum Brain Mapp. 35: 2754–2767.

Caspers J, Zilles K, Eickhoff SB, Schleicher A, Mohlberg H, Amunts K. 2013. Cytoarchitectonical analysis and probabilistic mapping of two extrastriate areas of the human posterior fusiform gyrus. Brain Struct Funct. 218:511–526.

Cohen L, Dehaene S, Naccache L, Lehericy S, Dehaene-Lambertz G, Henaff MA, Michel F. 2000. The visual word form area: spatial and temporal characterization of an initial stage of reading in normal subjects and posterior split-brain patients. Brain. 123(Pt 2):291–307.

Curcio CA, Allen KA. 1990. Topography of ganglion cells in human retina. J Comp Neurol. 300:5–25.

Dacey DM, Petersen MR. 1992. Dendritic field size and morphology of midget and parasol ganglion cells of the human retina. Proc Natl Acad Sci USA. 89:9666–9670.

Dehaene S, Cohen L. 2011. The unique role of the visual word form area in reading. Trends Cogn Sci. 15:254–262.

DiCarlo JJ, Cox DD. 2007. Untangling invariant object recognition. Trends Cogn Sci. 11:333–341.

Epstein R, Kanwisher N. 1998. A cortical representation of the local visual environment. Nature. 392:598–601.

Fischl B, Rajendran N, Busa E, Augustinack J, Hinds O, Yeo BT, Mohlberg H, Amunts K, Zilles K. 2008. Cortical folding patterns and predicting cytoarchitecture. Cereb Cortex. 18: 1973–1980.

Fischl B, Sereno MI, Tootell RB, Dale AM. 1999. High-resolution intersubject averaging and a coordinate system for the cortical surface. Hum Brain Mapp. 8:272–284.

Gaillard R, Naccache L, Pinel P, Clemenceau S, Volle E, Hasboun D, Dupont S, Baulac M, Dehaene S, Adam C, et al. 2006. Direct intracranial, FMRI, and lesion evidence for the causal role of left inferotemporal cortex in reading. Neuron. 50:191–204.

Gauthier I, Skudlarski P, Gore JC, Anderson AW. 2000. Expertise for cars and birds recruits brain areas involved in face recognition. Nat Neurosci. 3:191–197.

Gilaie-Dotan S, Nir Y, Malach R. 2008. Regionally-specific adaptation dynamics in human object areas. Neuroimage. 39: 1926–1937.

Glasser MF, Van Essen DC. 2011. Mapping human cortical areas in vivo based on myelin content as revealed by T1- and T2-weighted MRI. J Neurosci. 31:11597–11616.

Glezer LS, Jiang X, Riesenhuber M. 2009. Evidence for highly selective neuronal tuning to whole words in the "visual word form area". Neuron. 62:199–204.

Glezer LS, Riesenhuber M. 2013. Individual variability in location impacts orthographic selectivity in the "visual word form area". J Neurosci. 33:11221–11226.

Gomez J, Pestilli F, Witthoft N, Golarai G, Liberman A, Poltoratski S, Yoon J, Grill-Spector K. 2015. Functionally defined white matter reveals segregated pathways in human ventral temporal cortex associated with category-specific processing. Neuron. 85:216–227.

Greve DN, Van der Haegen L, Cai Q, Stufflebeam S, Sabuncu MR, Fischl B, Brysbaert M. 2013. A surface-based analysis of language lateralization and cortical asymmetry. J Cogn Neurosci. 25:1477–1492.

Grill-Spector K, Knouf N, Kanwisher N. 2004. The fusiform face area subserves face perception, not generic within-category identification. Nat Neurosci. 7:555–562.

Grill-Spector K, Malach R. 2004. The human visual cortex. Annu Rev Neurosci. 27:649–677.

Grill-Spector K, Weiner KS. 2014. The functional architecture of the ventral temporal cortex and its role in categorization. Nat Rev Neurosci. 15:536–548.

Gross CG, Rocha-Miranda CE, Bender DB. 1972. Visual properties of neurons in inferotemporal cortex of the Macaque. J Neurophysiol. 35:96–111.

Hasson U, Levy I, Behrmann M, Hendler T, Malach R. 2002. Eccentricity bias as an organizing principle for human high-order object areas. Neuron. 34:479–490.

Hinds O, Polimeni JR, Rajendran N, Balasubramanian M, Amunts K, Zilles K, Schwartz EL, Fischl B, Triantafyllou C. 2009. Locating the functional and anatomical boundaries of human primary visual cortex. Neuroimage. 46:915–922.

Hubel DH, Wiesel TN. 1977. Ferrier lecture. Functional architecture of macaque monkey visual cortex. Proc R Soc London B Biol Sci. 198:1–59.

Julian JB, Fedorenko E, Webster J, Kanwisher N. 2012. An algorithmic method for functionally defining regions of

interest in the ventral visual pathway. Neuroimage. 60: 2357–2364.
Kanwisher N, McDermott J, Chun MM. 1997. The fusiform face area: a module in human extrastriate cortex specialized for face perception. J Neurosci. 17:4302–4311.
Kay KN, Weiner KS, Grill-Spector K. 2015. Attention reduces spatial uncertainty in human ventral temporal cortex. Curr Biol. 25:595–600.
Kennedy H, Dehay C, Bullier J. 1986. Organization of the callosal connections of visual areas V1 and V2 in the macaque monkey. J Comp Neurol. 247:398–415.
Kravitz DJ, Saleem KS, Baker CI, Ungerleider LG, Mishkin M. 2013. The ventral visual pathway: an expanded neural framework for the processing of object quality. Trends Cogn Sci. 17:26–49.
Levy I, Hasson U, Avidan G, Hendler T, Malach R. 2001. Center-periphery organization of human object areas. Nat Neurosci. 4:533–539.
Lorenz S, Weiner KS, Caspers J, Mohlberg H, Schleicher A, Bludau S, Eickhoff SB, Grill-Spector K, Zilles K, Amunts K. 2015. Two new cytoarchitectonic areas on the human mid-fusiform gyrus. Cereb Cortex.
Megevand P, Groppe DM, Goldfinger MS, Hwang ST, Kingsley PB, Davidesco I, Mehta AD. 2014. Seeing scenes: topographic visual hallucinations evoked by direct electrical stimulation of the parahippocampal place area. J Neurosci. 34:5399–5405.
Nasr S, Echavarria CE, Tootell RB. 2014. Thinking outside the box: rectilinear shapes selectively activate scene-selective cortex. J Neurosci. 34:6721–6735.
Nasr S, Liu N, Devaney KJ, Yue X, Rajimehr R, Ungerleider LG, Tootell RB. 2011. Scene-selective cortical regions in human and nonhuman primates. J Neurosci. 31:13771–13785.
Nestares O, Heeger DJ. 2000. Robust multiresolution alignment of MRI brain volumes. Magn Reson Med. 43:705–715.
Osher DE, Saxe RR, Koldewyn K, Gabrieli JD, Kanwisher N, Saygin ZM. 2016. Structural connectivity fingerprints predict cortical selectivity for multiple visual categories across cortex. Cereb Cortex. 26:1668–1683.
Parvizi J, Jacques C, Foster BL, Withoft N, Rangarajan V, Weiner KS, Grill-Spector K. 2012. Electrical stimulation of human fusiform face-selective regions distorts face perception. J Neurosci. 32: 14915–14920.
Peelen MV, Downing PE. 2005a. Selectivity for the human body in the fusiform gyrus. J Neurophysiol. 93:603–608.
Peelen MV, Downing PE. 2005b. Within-subject reproducibility of category-specific visual activation with functional MRI. Hum Brain Mapp. 25:402–408.
Puce A, Allison T, Gore JC, McCarthy G. 1995. Face-sensitive regions in human extrastriate cortex studied by functional MRI. J Neurophysiol. 74:1192–1199.
Rangarajan V, Hermes D, Foster BL, Weiner KS, Jacques C, Grill-Spector K, Parvizi J. 2014. Electrical stimulation of the left and right human fusiform gyrus causes different effects in conscious face perception. J Neurosci. 34:12828–12836.
Reckfort J, Wiese H, Pietrzyk U, Zilles K, Amunts K, Axer M. 2015. A multiscale approach for the reconstruction of the fiber architecture of the human brain based on 3D-PLI. Front Neuroanat. 9:118.
Saygin ZM, Osher DE, Koldewyn K, Reynolds G, Gabrieli JD, Saxe RR. 2012. Anatomical connectivity patterns predict face selectivity in the fusiform gyrus. Nat Neurosci. 15:321–327.
Schleicher A, Amunts K, Geyer S, Kowalski T, Schormann T, Palomero-Gallagher N, Zilles K. 2000. A stereological approach to human cortical architecture: identification and delineation of cortical areas. J Chem Neuroanat. 20:31–47.
Schwarzlose RF, Baker CI, Kanwisher N. 2005. Separate face and body selectivity on the fusiform gyrus. J Neurosci. 25: 11055–11059.
Silson EH, Chan AW, Reynolds RC, Kravitz DJ, Baker CI. 2015. A retinotopic basis for the division of high-level scene processing between lateral and ventral human occipitotemporal cortex. J Neurosci. 35:11921–11935.
Smith GE. 1907. A new topographical survey of the human cerebral cortex, being an account of the distribution of the anatomically distinct cortical areas and their relationship to the cerebral sulci. J Anat Physiol. 41:237–254.
Spiridon M, Fischl B, Kanwisher N. 2006. Location and spatial profile of category-specific regions in human extrastriate cortex. Hum Brain Mapp. 27:77–89.
Stigliani A, Weiner KS, Grill-Spector K. 2015. Temporal processing capacity in high-level visual cortex is domain specific. J Neurosci. 35:12412–12424.
Van Essen DC. 2003. Organization of visual areas in macaque and human cerebral cortex. In: Chalupa L, Werner J, editors. Visual Neurosciences, Cambridge MA, USA: MIT Press.
Van Essen DC, Anderson CH, Felleman DJ. 1992. Information processing in the primate visual system: an integrated systems perspective. Science. 255:419–423.
Van Essen DC, Glasser MF, Dierker DL, Harwell J, Coalson T. 2012. Parcellations and hemispheric asymmetries of human cerebral cortex analyzed on surface-based atlases. Cereb Cortex. 22:2241–2262.
Van Essen DC, Zeki SM. 1978. The topographic organization of rhesus monkey prestriate cortex. J Physiol. 277:193–226.
von Economo C, Koskinas GN. 1925. Atlas of cytoarchitectonics of the adult human cerebral cortex. Berlin, Germany: Springer.
Wandell BA. 2016. Clarifying human white matter. Annu Rev Neurosci. 39:103–128.
Wandell BA, Chial S, Backus BT. 2000. Visualization and measurement of the cortical surface. J Cogn Neurosci. 12:739–752.
Wandell BA, Winawer J. 2015. Computational neuroimaging and population receptive fields. Trends Cogn Sci. 19: 349–357.
Weiner KS, Barnett M, Witthoft N, Golarai G, Stigliani A, Gomez J, Natu V, Amunts K, Zilles K, Grill-Spector K Defining the parahippocampal place area from cortical folding and probabilistic predictions. Neuroimage. Under review.
Weiner KS, Golarai G, Caspers J, Chuapoco MR, Mohlberg H, Zilles K, Amunts K, Grill-Spector K. 2014. The mid-fusiform sulcus: a landmark identifying both cytoarchitectonic and functional divisions of human ventral temporal cortex. Neuroimage. 84:453–465.
Weiner KS, Grill-Spector K. 2010. Sparsely-distributed organization of face and limb activations in human ventral temporal cortex. Neuroimage. 52:1559–1573.
Weiner KS, Grill-Spector K. 2011. Not one extrastriate body area: using anatomical landmarks, hMT+, and visual field maps to parcellate limb-selective activations in human lateral occipitotemporal cortex. Neuroimage. 56:2183–2199.
Weiner KS, Grill-Spector K. 2012. The improbable simplicity of the fusiform face area. Trends Cogn Sci. 16:251–254.
Weiner KS, Sayres R, Vinberg J, Grill-Spector K. 2010. fMRI-adaptation and category selectivity in human ventral temporal cortex: Regional differences across time scales. J Neurophysiol. 103:3349–3365.

Weiner KS, Yeatman JD, Wandell BA. 2016. The posterior arcuate fasciculus and the vertical occipital fasciculus. Cortex. pii: (16)30050-8. do:S0010-9452.

Weiner KS, Zilles K. 2016. The anatomical and functional specialization of the fusiform gyrus. Neuropsychologia. 83: 48–62.

Yeatman JD, Rauschecker AM, Wandell BA. 2012. Anatomy of the visual word form area: adjacent cortical circuits and long-range white matter connections. Brain Lang. 125: 146–155.

Zangenehpour S, Chaudhuri A. 2005. Patchy organization and asymmetric distribution of the neural correlates of face processing in monkey inferotemporal cortex. Curr Biol. 15: 993–1005.

Zilles K, Amunts K. 2010. Centenary of Brodmann's map—conception and fate. Nat Rev Neurosci. 11:139–145.